Structural basis for ligase-specific conjugation of linear ubiquitin chains by HOIP.

Stieglitz, B; Rana, RR; Koliopoulos, MG; Morris-Davies, AC; Schaeffer, V; Christodoulou, E; Howell, S; Brown, NR; Dikic, I; Rittinger, K

Published in final edited form as:
Nature. 2013 November 21; 503(7476): 422–426. doi:10.1038/nature12638.

Structural basis for ligase-specific conjugation of linear ubiquitin chains by HOIP

Benjamin Stieglitz[#1], **Rohini R. Rana**[#1], **Marios G. Koliopoulos**[1], **Aylin C. Morris-Davies**[1], **Veronique Schaeffer**[2], **Evangelos Christodoulou**[1], **Steven Howell**[1], **Nicholas R. Brown**[1], **Ivan Dikic**[2], and **Katrin Rittinger**[1,*]

[1]Division of Molecular Structure, MRC-National Institute for Medical Research, The Ridgeway, London NW7 1AA, UK

[2]Institute of Biochemistry II, Goethe University, School of Medicine, Theodor-Stern-Kai 7, D-60590 Frankfurt (Main), Germany

[#] These authors contributed equally to this work.

Abstract

Linear ubiquitin chains are important regulators of cellular signaling pathways that control innate immunity and inflammation through NF-κB activation and protection against TNFα-induced apoptosis[1-5]. They are synthesized by HOIP, which belongs to the RBR (RING-between-RING) family of E3 ligases and is the catalytic component of LUBAC (linear ubiquitin chain assembly complex), a multi-subunit E3 ligase[6]. RBR family members act as RING/HECT hybrids, employing RING1 to recognize ubiquitin-loaded E2 while a conserved cysteine in RING2 subsequently forms a thioester intermediate with the transferred or "donor" ubiquitin[7]. Here we report the crystal structure of the catalytic core of HOIP in its apo form and in complex with ubiquitin. The C-terminal portion of HOIP adopts a novel fold that, together with a zinc finger, forms an ubiquitin-binding platform which orients the acceptor ubiquitin and positions its α-amino group for nucleophilic attack on the E3~ubiquitin thioester. The carboxy-terminal tail of a second ubiquitin molecule is located in close proximity to the catalytic cysteine providing a unique snapshot of the ubiquitin transfer complex containing both donor and acceptor ubiquitin. These interactions are required for activation of the NF-kB pathway *in vivo* and explain the determinants of linear ubiquitin chain specificity by LUBAC.

Keywords

E3 ubiquitin ligase; linear ubiquitin chains; structure; mechanism; ubiquitination

[*]Correspondence to: katrin.rittinger@nimr.mrc.ac.uk.

Author contributions B.S., R.R.R. and M.G.K. purified proteins and carried out structural and biochemical analysis, A.C.M.-D. and N.R.B. purified proteins and carried out biochemical analysis, V.S. carried out *in vivo* studies, E.C. produced expression plasmids, S.H. carried out MS analysis, I.D. coordinated experimental work and contributed ideas, K.R. contributed to structural analysis and wrote the paper. All authors contributed to data analysis, experimental design and paper writing.

Supplementary Information is linked to the online version of the paper at www.nature.com/nature.

Author Information Coordinates and structure factors were deposited in the protein Data Bank under accession codes 4LJQ (apo $HOIP_{CBR-C}$ structure), 4LJO (WT $HOIP_{CBR-C}$/ubiquitin complex) and 4LJP (H889A $HOIP_{CBR-C}$/ubiquitin complex).

The authors declare no competing financial interests.

Europe PMC Funders Author Manuscripts

Protein modification with ubiquitin is a key mechanism for the regulation of numerous cellular functions[8]. The transfer of ubiquitin onto a substrate is catalyzed by E3 ligases, which can be classified into RING, HECT and RBR families[9-13]. Two LUBAC subunits contain RBR domains. However, HOIP constitutes the catalytic center and its RBR domain-containing C-terminal region ($HOIP_{RBR-C}$) is sufficient to synthesise linear ubiquitin chains, regardless of E2 (Fig. 1a)[6,14,15]. Although the RING1 domain of RBRs is assumed to be the primary binding site for E2s, we show that a HOIP construct containing only the catalytic cysteine-carrying RING2 plus a C-terminal extension ($HOIP_{CBR-C}$) still forms linear ubiquitin chains, at a ~7-fold slower rate than $HOIP_{RBR-C}$ (Fig. 1b and Extended Data Fig. 1)[7,15]. Hence $HOIP_{CBR-C}$ constitutes the minimal catalytic core. We have determined the crystal structure of this catalytic core in its apo form at 2.4 Å and in complex with ubiquitin at 1.6 Å resolution (Extended Data Table 1). $HOIP_{CBR-C}$ consists of 7 α-helices and 4 zinc-binding modules and its overall topology appears distinct from other structures (Figs. 1c-e and Extended Data Fig. 2). The helical region forms an elongated structural unit that acts as a platform, the “helical base”, to support the zinc-binding modules. The RING2 region of RBRs has recently been shown to adopt the IBR domain fold in auto-inhibited Parkin and HHARI[16-21]. This fold is preserved in the structure of active $HOIP_{CBR-C}$ (Fig. 1c-e and Extended Data Fig. 3) and based on this structural and high sequence conservation we suggest it be renamed CBR (for “catalytic IBR”). Remarkably, the second zinc-binding site of the CBR of $HOIP_{CBR-C}$ has a zinc finger (ZF1) inserted between the second and third Zn^{2+}-coordinating residues. A fourth zinc-binding site is located between helices α3 and α4 (ZF2) and anchors the β-hairpin that is positioned close to the CBR.

In the $HOIP_{CBR-C}$/ubiquitin complex, ubiquitin makes contacts with residues from the helical base and ZF1 (Fig. 2 and Extended Data Fig.4). No major conformational changes occur upon complex formation, although some disordered regions of apo $HOIP_{CBR-C}$ become ordered (Extended Data Fig. 2d). The ubiquitin bound by the helical base and ZF1 constitutes the acceptor ubiquitin: its α-amino-group of M1 is located 3.5 Å away from the thioester-forming C885, poised for nucleophilic attack (Fig. 2). Strikingly, the C-terminal G76 of ubiquitin from a symmetry-related molecule is oriented such that its carboxylate points into the active site of $HOIP_{CBR-C}$ sufficiently close to C885 to promote thioester formation. Thus, the molecular arrangement within the crystal lattice mimics the biologically relevant ubiquitin transfer complex with the donor and acceptor ubiquitin in an orientation consistent with linear chain synthesis (Fig. 2 and Extended Data Fig.4). Unexpectedly, we found additional electron density in the active site, which we interpret as a zinc ion. However, mass spectrometry, combined with structural and biochemical analysis show that ubiquitin chain synthesis is not a zinc-dependent process (Extended Data Figs. 2b and 5).

$HOIP_{CBR-C}$ employs residues from helices α2 and α6 in the helical base to contact T14, E16, D32 and K33 of the acceptor ubiquitin, while ZF1 rests against helix α1 and the preceding loop (Fig. 3a and Extended Data Fig. 6a) ensuring that the N-terminal amino group is positioned closest to the active site and thus specifying linear chain synthesis. Notably, the side chain of M1 points away from the active site indicating that its selection is stereochemically driven. To analyze the role of individual residues in ligase activity we used a combination of steady state and single-turnover assays (Fig. 3c, d and Extended Data Fig. 6). Contributions from the helical base are crucial for ubiquitin chain synthesis, especially R935 and D936, but their mutation does not impede thioester formation (Extended Data Fig. 6c). In ubiquitin the most severe effect was seen upon K33 mutation, while E16A and D32A showed reduced activity. No point mutation could be identified at the ZF1-ubiquitin interface that reduced chain synthesis, however, ZF1 deletion results in an almost complete loss of activity (Fig. 3c). This impairment is not caused by protein misfolding since ubiquitin-thioester formation is unaffected (Extended Data Fig. 6c). Instead, ZF1 deletion

abolishes transfer of the donor onto the acceptor ubiquitin. These data suggest that the helical base constitutes the primary binding site for the acceptor ubiquitin which is further supported by ZF1.

$HOIP_{CBR-C}$ residues that contact the acceptor ubiquitin are located in a region termed the "linear ubiquitin chain determining region" (LDD, residues 910-1,082)[15]. Our structure now shows that this is not an independent ubiquitin binding-module, but together with the CBR forms a super-domain which contacts donor and acceptor ubiquitin to create a platform that promotes linear chain synthesis.

Contacts between $HOIP_{CBR-C}$ and the donor ubiquitin primarily involve the C-terminal tail of ubiquitin which is guided towards the active site through a channel created by the N-terminal anti-parallel β-strands of the CBR and a β-hairpin formed by βF and βE (Fig. 2 and 3b). These structural elements restrict tail mobility ensuring that the carboxylate of G76 is located next to the catalytic cysteine. Contacts between Q974 and D983 in the β-hairpin and R72 and R74 from ubiquitin are crucial for donor ubiquitin binding (Fig. 3b-d and Extended Data Fig. 6). Interestingly the β-hairpin is largely disordered in the apo structure suggesting that, together with the CBR, it could act as a flexible clamp locking the donor ubiquitin into place. Ubiquitin is further sandwiched by the N-terminal β-sheets of the CBR that form a hydrophobic pocket which accommodates L73 and contacts L71. Mutation of either results in severe loss of activity (Figs. 3c). Most of the hydrophobic residues contacting L71 and L73 are conserved in CBRs, indicating that this mode of donor ubiquitin presentation to the substrate may be a general property of RBRs (Extended Data Fig.3).

To confirm that the mechanism of linear ubiquitin chain synthesis identified in $HOIP_{CBR-C}$ is maintained in LUBAC, we carried out *in vitro* ubiquitination assays with the heterotrimeric complex. While the activity of LUBAC is lower than of isolated $HOIP_{RBR-C}$, possibly due to regulatory roles of ubiquitin binding domains present in all 3 subunits, there is a strong correlation with the trends seen in ubiquitination assays using different ubiquitin mutants, indicating that domains outside $HOIP_{RBR-C}$ do not affect chain linkage specificity (Extended Data Fig. 7). To validate our conclusions in a physiological context, we carried out *in vivo* NF-kB activation and p65 nuclear translocation assays employing HOIP mutants shown to affect interaction with the donor (D983A) and acceptor (R935A, D936A) ubiquitin. Consonant with our structural and biochemical data these mutants reduced NF-κB signalling and p65 nuclear translocation upon overexpression (Figs. 3e, f) without impairing complex formation between LUBAC subunits (Extended Data Fig. 7).

Ubiquitin chain synthesis involves the nucleophilic attack of an amino group from a lysine or the N-terminus of ubiquitin onto an ubiquitin-thioester formed by the E2 or HECT-type E3s. The reaction requires a general base to deprotonate the nucleophile and a mechanism to stabilize the transition state[22-24]. In the $HOIP_{CBR-C}$/ubiquitin complex, H887 of $HOIP_{CBR-C}$ forms a hydrogen bond with M1 of ubiquitin suggesting it could activate the incoming α-amino group or stabilize the transition state. To test its contribution to catalysis, we measured the activity of H887A which was reduced over 1000-fold at 15°C. This is due to lack of transfer onto the acceptor ubiquitin rather than impairment of thioester formation (Figs. 3d and 4a). Thus H887 is not required for transthiolation from E2 to E3. To further characterize its function, we tested if activity could be rescued at increased pH, which would aid deprotonation of the nucleophile. Indeed, ubiquitin transfer assays with H887A showed that activity could be restored at pH 9.0, although this required higher temperature and substrate concentrations (Fig. 4b). Accordingly, enzyme activity is lost below pH 6.0, the approximate pKa of an imidazole sidechain (Extended Data Fig. 8). Taken together, these observations support a model for ubiquitin transfer in which H887 acts as a general base to activate the nucleophile (Fig. 4c). This mechanism is maintained *in vivo* as indicated by the

reduction of NF-κB activation and p65 translocation by the H887A mutant (Figs. 3e, f). Notably, a histidine in this position is conserved in a number of RBRs and has recently been shown to be important for activity in Parkin and HHARI[16,17,20], suggesting that the mechanism of nucleophile activation may be conserved.

The $HOIP_{CBR-C}$/ubiquitin complex structure presented here provides the first insights into how an E3 ligase directs the synthesis of specific ubiquitin chains: a non-covalent ubiquitin binding site orients the acceptor so that only the α-amino group of M1 is presented to the active site, similar to the mechanism used by linkage specific E2s [24-26] (Extended Data Fig. 9). M1 is part of a β-sheet and less flexible than the ε-amino group of lysine, potentially explaining why HOIP has evolved a single structural unit that integrates the CBR domain with the donor and acceptor ubiquitin binding regions. Comparison of CBR structures from active HOIP with auto-inhibited Parkin and HHARI suggests that the overall mechanism of donor ubiquitin presentation is conserved in the RBR family[16-21]. Further studies are now required to reveal the mechanism that promotes formation of the active ligase complex and explain how chain linkage specificity is achieved in other RBR ligases.

METHODS

Cloning, expression and protein purification

Cloning, expression and purification of Ube1, UbcH5A (UBE2D1), $HOIP_{RBR-C}$ and mutants thereof, HOIP (residues 300-1072), HOIL-1L, SHARPIN and His_6-M1C-ubiquitin have been described[14]. $HOIP_{CBR-C}$ was expressed and purified using the same procedure as for $HOIP_{RBR-C.}$ Point mutations were generated using the QuikChange site-directed mutagenesis kit (Stratagene). The ZF1 of HOIP (residues 906-923) was deleted in $HOIP_{RBR-C}$ and replaced with the sequence PG using Overlap Extension-PCR[27]. Untagged ubiquitin and mutants were prepared according to Pickart and Raasi[28]. Seleno-methionine (SeMet)-substituted proteins were produced by standard procedures. Ubiquitin used for crystallization was purchased from Sigma and further purified by gel filtration. All plasmids were verified by DNA sequencing. Protein molecular mass was verified by electrospray ionization mass-spectrometry. The fold of all proteins was analyzed by circular dichroism spectroscopy.

Ubiquitination assays

Ubiquitination assays were performed using 1 μM E1, 5 μM UbcH5A, 5 μM HOIP (or 5μM each: HOIP residues 300-1072, HOIL-1L and SHARPIN) and 200 μM ubiquitin[14]. Reactions were incubated at 30°C for 1 h and samples taken at 0, 5, 15, 30, 60 min ($HOIP_{RBR-C}$) or 0.5, 1, 2, 4 hrs ($HOIP_{CBR-C}$). Reactions were stopped by addition of SDS sample buffer containing 40 mM N-Ethylmaleimide (NEM). For LUBAC assays an additional precipitation step using 50 mM NaAc, pH 4.0/60°C was introduced. Samples were analyzed by SDS-PAGE and visualized using Coomassie Brilliant blue.

Thioester formation and ubiquitin transfer assays

Labelling of His_6-Cys-ubiquitin with Cy5-Maleimide mono-Reactive Dye (GE Healthcare) and transfer assays were carried out as described with minor modifications[14]. 1 μM Cy5-ubiquitin was mixed with 2 μM E1 and 1 mM ATP. After 5 min 10 μM UbcH5A was added and after further 5 min 20 μM $HOIP_{RBR-C}$. To monitor ubiquitin transfer, 10 μM Ub-His_6 was added. Samples were taken before each addition and analysed by SDS-PAGE in the absence and presence of DTT.

Single-turnover FRET assays

UbcH5A was charged with Cy5-labeled linear di-ubiquitin and purified by gel filtration. 0.3 μM or 3.0 μM (for pH-dependent assays) of E2~thioester was mixed with 0.3μM or 3.0 μM Cy3-labeled linear di-ubiquitin. After addition of 3.0 μM of $HOIP_{RBR-C}$ or $HOIP_{CBR-C}$, tetra-ubiquitin chain synthesis was observed by fluorescence resonance energy transfer (FRET) between Cy3 and Cy5 using excitation and emission wavelengths of 540 nm and 670 nm, respectively. Samples were incubated at 15° C in 50 mM HEPES pH 7.4, 150 mM NaCl, or at 25°C for pH-dependent assays using phosphate (pH 6-8) and CHES (pH 8.5-10.0) buffers. Data were analyzed by single exponential curve fitting. Data for constructs with very low activity were analyzed by linear regression and a rate constant was calculated by dividing the obtained slope by the amplitude taken from the $HOIP_{RBR-C}$ WT measurement. All measurements were carried out in duplicate or triplicate and mean values are given.

Luciferase and p65 translocation assays

HeLa cells were transfected with pCMV-FLAG-HOIP (WT, H887A, R935A, D936A, D983A), pcDNA5-HA-SHARPIN, pNF-κB-Luc (Stratagene) and β-GAL plasmids using Genejuice. After 36 hrs of transfection, lysates were prepared and subjected to luciferase assays following the manufacturer's protocol (Roche). Internal control was measured by β-Gal activity using its substrate (Roche). Three independent experiments were performed using triplicate samples in each experiment. For translocation assays HeLa cells were fixed and stained for p65 (SantaCruz, sc-372) and HA-SHARPIN (Covance, MMS-101P). The total number of cells showing nuclear staining of p65 was counted and normalized to the total number of cells expressing HA-SHARPIN to determine the percentage of translocation. Three independent experiments were performed using triplicate samples in each experiment. Results were analyzed by ANOVA1 followed by Tukey post-tests and are presented as average plus s.e.m. ** $p<0.01$; *** $p<0.001$ compared to WT HOIP.

Co-immunoprecipitation assays

HeLa cells were transfected with pCMV-FLAG-HOIP, pcDNA5-HA-SHARPIN and pcDNA5-HA-HOIL-1L plasmids. After 36h FLAG-HOIP immunoprecipitation was performed using anti-FLAG M2 affinity gel (Sigma). The samples were subsequently probed for FLAG-HOIP, HA-SHARPIN and HA-HOIL-1L.

Crystallisation of apo $HOIP_{CBR-C}$ and the ubiquitin complex

Crystallisation trials with $HOIP_{CBR-C}$ and its SeMet-derivative were set-up at 9.5 mg/ml using an Oryx crystallisation robot. Initial hits were optimised by sitting drop vapour diffusion at 18 °C with a reservoir solution containing 100 mM Tris pH 8.5, 800 mM LiCl and 20 % PEG 12000. Crystals were flash-frozen in the reservoir solution containing 30 % glycerol. $HOIP_{CBR-C}$ (0.6 mM) and ubiquitin were mixed at 1:2 and 1:3 molar ratios. Initial crystals were obtained in the Morpheus screen and optimised in hanging-drops with reservoir solution containing 0.1 M carboxylic acids, buffer system 1 (0.1 M) pH 6.5, 30% P550 MME _P20K. Crystals were flash-frozen in the reservoir solution. Crystals of mutant $HOIP_{CBR-C}$ H899A with ubiquitin were grown under the same conditions as the wild-type protein.

Data collection and structure determination

Crystals of $HOIP_{CBR-C}$ diffracted to 2.44 Å. A data set was collected on beamline IO3 (λ=0.9798 Å) at the Diamond Light Source (Oxford, UK) and processed using XDS[29]. The structure was solved by single wavelength anomalous dispersion phasing using the SeMet-derivative of $HOIP_{CBR-C}$. Heavy atom search, density modification, and initial model

building was performed using Phenix AutoSol[30]. Diffraction data for crystals of $HOIP_{CBR-C}$ (WT) and $HOIP_{CBR-C}$ (H889A) in complex with ubiquitin were collected at beamline IO4 (λ=1.282 Å), and IO4-1 (λ=0.9163 Å), respectively. Data were reduced using Xia2 from the CCP4 suite and the structure of the complex was determined by molecular replacement in Phaser[31] using the apo structure and ubiquitin (1UBQ.pdb) as search models. All models were iteratively improved by manual building in Coot[32] and refined using REFMAC5[33] and Phenix[30]. The stereochemistry of the final models was 05analyzed with Procheck. The model of apo $HOIP_{CBR-C}$ has 94.8% of residues in favored regions, 4.2% in allowed regions and 1% outliers. The final models of WT $HOIP_{CBR-C}$/ubiquitin and $HOIP_{CBR-C}$ H889A/ubiquitin have 97.6% and 95.5% of residues in the favored regions of Ramachandran plot, respectively. Structural figures were prepared in Pymol.

Mass spectrometry

For zinc content analysis by native mass spectrometry, purified proteins were dialysed at 4 °C against 20 mM ammonium acetate pH 7.4. Molecular mass was determined by electrospray ionisation (ESI) on a microTOFQ electrospray mass spectrometer (Bruker Daltonics, Coventry, UK). Protein was infused into the mass spectrometer at 3 μl/min using an electrospray voltage of 4.5 kV. Inductively coupled plasma mass spectrometry (ICP-MS) was used to determine the concentration of Ca and Zn (as ^{44}Ca and ^{66}Zn) in the protein samples using an Agilent 7700x instrument in Helium (He) collision mode.

Analytical ultracentrifugation

Sedimentation velocity experiments were performed in a Beckman XL-I analytical ultracentrifuge. Samples were dialyzed against the buffer blank, 20 mM Tris-HCl, 150 mM NaCl, 0.5mM TCEP, pH 7.5. Centrifugation was performed at 50,000 rpm and 293 K in an An50-Ti rotor at 125 μM sample concentrations. Data were analyzed in terms of the size distribution function C(S) using the program SEDFIT[34].

Supplementary Material

Refer to Web version on PubMed Central for supplementary material.

Acknowledgments

We thank Stanislav Strekopytov, Natural History Museum London, for ICP-MS experiments, Ian Taylor, for help with AUC, Lesley Haire for help with crystallization, Steve Martin for CD spectroscopy, Sarah Caswell for help with cloning, Caroline Bayart for technical assistance, Phil Walker for data collection and the Diamond Light Source for synchrotron access. We are grateful to Steve Smerdon for discussions and advice. This work was supported by the Medical Research Council, grant U117565398 and Wellcome Grant 094112/Z/10/Z to K.R. and the European Research Council (ERC) under the European Union's Seventh Framework Programme (FP7/2007-2013) and ERC grant agreement 250241-LineUb to I.D.

References

1. Walczak H, Iwai K, Dikic I. Generation and physiological roles of linear ubiquitin chains. BMC Biol. 2012; 10:23. doi:10.1186/1741-7007-10-23. [PubMed: 22420778]
2. Tokunaga F, et al. Involvement of linear polyubiquitylation of NEMO in NF-kappaB activation. Nat Cell Biol. 2009; 11:123–132. doi:ncb1821 [pii] 10.1038/ncb1821. [PubMed: 19136968]
3. Ikeda F, et al. SHARPIN forms a linear ubiquitin ligase complex regulating NF-kappaB activity and apoptosis. Nature. 2011; 471:637–641. doi:10.1038/nature09814. [PubMed: 21455181]
4. Tokunaga F, Iwai K. LUBAC, a novel ubiquitin ligase for linear ubiquitination, is crucial for inflammation and immune responses. Microbes Infect. 2012 doi:10.1016/j.micinf.2012.01.011.
5. Gerlach B, et al. Linear ubiquitination prevents inflammation and regulates immune signalling. Nature. 2011; 471:591–596. doi:10.1038/nature09816. [PubMed: 21455173]

6. Kirisako T, et al. A ubiquitin ligase complex assembles linear polyubiquitin chains. EMBO J. 2006; 25:4877–4887. doi:7601360 [pii] 10.1038/sj.emboj.7601360. [PubMed: 17006537]
7. Wenzel DM, Lissounov A, Brzovic PS, Klevit RE. UBCH7 reactivity profile reveals parkin and HHARI to be RING/HECT hybrids. Nature. 2011; 474:105–108. doi:10.1038/nature09966. [PubMed: 21532592]
8. Pickart CM, Fushman D. Polyubiquitin chains: polymeric protein signals. Curr Opin Chem Biol. 2004; 8:610–616. doi:S1367-5931(04)00141-3 [pii] 10.1016/j.cbpa.2004.09.009. [PubMed: 15556404]
9. Deshaies RJ, Joazeiro CA. RING domain E3 ubiquitin ligases. Annu Rev Biochem. 2009; 78:399–434. doi:10.1146/annurev.biochem.78.101807.093809. [PubMed: 19489725]
10. Huibregtse JM, Scheffner M, Beaudenon S, Howley PM. A family of proteins structurally and functionally related to the E6-AP ubiquitin-protein ligase. Proc Natl Acad Sci U S A. 1995; 92:2563–2567. [PubMed: 7708685]
11. Wang M, Pickart CM. Different HECT domain ubiquitin ligases employ distinct mechanisms of polyubiquitin chain synthesis. EMBO J. 2005; 24:4324–4333. doi:7600895 [pii] 10.1038/sj.emboj.7600895. [PubMed: 16341092]
12. Eisenhaber B, Chumak N, Eisenhaber F, Hauser MT. The ring between ring fingers (RBR) protein family. Genome Biol. 2007; 8:209. doi:10.1186/gb-2007-8-3-209. [PubMed: 17367545]
13. Wenzel DM, Klevit RE. Following Ariadne's thread: a new perspective on RBR ubiquitin ligases. BMC Biol. 2012; 10:24. doi:10.1186/1741-7007-10-24. [PubMed: 22420831]
14. Stieglitz B, Morris-Davies AC, Koliopoulos MG, Christodoulou E, Rittinger K. LUBAC synthesizes linear ubiquitin chains via a thioester intermediate. EMBO reports. 2012; 13:840–846. doi:10.1038/embor.2012.105. [PubMed: 22791023]
15. Smit JJ, et al. The E3 ligase HOIP specifies linear ubiquitin chain assembly through its RING-IBR-RING domain and the unique LDD extension. The EMBO journal. 2012; 31:3833–3844. doi:10.1038/emboj.2012.217. [PubMed: 22863777]
16. Trempe JF, et al. Structure of Parkin Reveals Mechanisms for Ubiquitin Ligase Activation. Science. 2013; 340:1451–1455. doi:10.1126/science.1237908. [PubMed: 23661642]
17. Wauer T, Komander D. Structure of the human Parkin ligase domain in an autoinhibited state. The EMBO journal. 2013; 32:2099–2112. doi:10.1038/emboj.2013.125. [PubMed: 23727886]
18. Spratt DE, et al. A molecular explanation for the recessive nature of parkin-linked Parkinson's disease. Nat Commun. 2013; 4:1983. doi:10.1038/ncomms2983. [PubMed: 23770917]
19. Riley BE, et al. Structure and function of Parkin E3 ubiquitin ligase reveals aspects of RING and HECT ligases. Nat Commun. 2013; 4:1982. doi:10.1038/ncomms2982. [PubMed: 23770887]
20. Duda DM, et al. Structure of HHARI, a RING-IBR-RING Ubiquitin Ligase: Autoinhibition of an Ariadne-Family E3 and Insights into Ligation Mechanism. Structure. 2013; 21:1030–1041. doi:10.1016/j.str.2013.04.019. [PubMed: 23707686]
21. Beasley SA, Hristova VA, Shaw GS. Structure of the Parkin in-between-ring domain provides insights for E3-ligase dysfunction in autosomal recessive Parkinson's disease. Proc Natl Acad Sci U S A. 2007; 104:3095–3100. doi:104/9/3095 [pii] 10.1073/pnas.0610548104. [PubMed: 17360614]
22. Yunus AA, Lima CD. Lysine activation and functional analysis of E2-mediated conjugation in the SUMO pathway. Nature structural & molecular biology. 2006; 13:491–499. doi:10.1038/nsmb1104.
23. Wu PY, et al. A conserved catalytic residue in the ubiquitin-conjugating enzyme family. The EMBO journal. 2003; 22:5241–5250. doi:10.1093/emboj/cdg501. [PubMed: 14517261]
24. Wickliffe KE, Lorenz S, Wemmer DE, Kuriyan J, Rape M. The mechanism of linkage-specific ubiquitin chain elongation by a single-subunit E2. Cell. 2011; 144:769–781. doi:10.1016/j.cell.2011.01.035. [PubMed: 21376237]
25. Eddins MJ, Carlile CM, Gomez KM, Pickart CM, Wolberger C. Mms2-Ubc13 covalently bound to ubiquitin reveals the structural basis of linkage-specific polyubiquitin chain formation. Nat Struct Mol Biol. 2006; 13:915–920. doi:nsmb1148 [pii] 10.1038/nsmb1148. [PubMed: 16980971]

26. Petroski MD, Deshaies RJ. Mechanism of lysine 48-linked ubiquitin-chain synthesis by the cullin-RING ubiquitin-ligase complex SCF-Cdc34. Cell. 2005; 123:1107–1120. doi:10.1016/j.cell.2005.09.033. [PubMed: 16360039]

References

27. Higuchi R, Krummel B, Saiki RK. A general method of in vitro preparation and specific mutagenesis of DNA fragments: study of protein and DNA interactions. Nucleic Acids Res. 1988; 16:7351–7367. [PubMed: 3045756]

28. Raasi S, Pickart CM. Ubiquitin chain synthesis. Methods Mol Biol. 2005; 301:47–55. doi:10.1385/1-59259-895-1:047. [PubMed: 15917625]

29. Kabsch W. Xds. Acta Crystallogr D Biol Crystallogr. 2010; 66:125–132. doi:10.1107/S0907444909047337. [PubMed: 20124692]

30. Adams PD, et al. PHENIX: a comprehensive Python-based system for macromolecular structure solution. Acta Crystallogr D Biol Crystallogr. 2010; 66:213–221. doi:10.1107/S0907444909052925. [PubMed: 20124702]

31. McCoy AJ, et al. Phaser crystallographic software. J Appl Crystallogr. 2007; 40:658–674. doi:10.1107/S0021889807021206. [PubMed: 19461840]

32. Emsley P, Cowtan K. Coot: model-building tools for molecular graphics. Acta Crystallogr D Biol Crystallogr. 2004; 60:2126–2132. doi:10.1107/S0907444904019158. [PubMed: 15572765]

33. Murshudov GN, Vagin AA, Dodson EJ. Refinement of macromolecular structures by the maximum-likelihood method. Acta Crystallogr D Biol Crystallogr. 1997; 53:240–255. doi:10.1107/S0907444996012255. [PubMed: 15299926]

34. Brown PH, Schuck P. Macromolecular size-and-shape distributions by sedimentation velocity analytical ultracentrifugation. Biophys J. 2006; 90:4651–4661. doi:10.1529/biophysj.106.081372. [PubMed: 16565040]

Europe PMC Funders Author Manuscripts

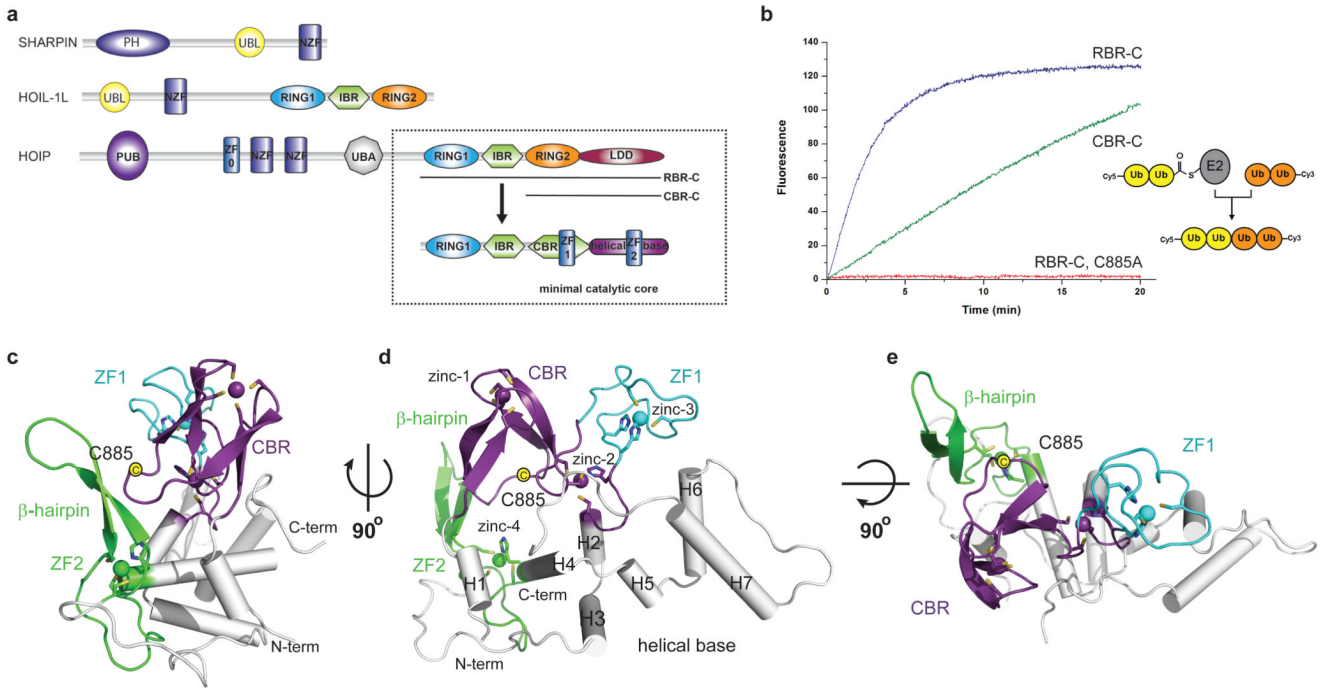

Fig. 1. Structure of the catalytic core of HOIP

a, Composition of LUBAC. Boxed: the crystallized catalytic core $HOIP_{CBR-C}$, biochemical assays employed $HOIP_{RBR-C}$. Below, schematic of new elements identified: CBR, ZF1, ZF2 and helical base. **b,** Single turnover assays showing that lack of RING1 reduces activity 6.8-fold ($HOIP_{CBR-C}$, 0.050 min^{-1} versus $HOIP_{RBR-C}$, 0.341 min^{-1}). **c-e,** Ribbon representation of $HOIP_{CBR-C}$ with the helical base in grey, CBR in purple, ZF1 in cyan and ZF2 and β-hairpin in green, zinc ions as spheres, coordinating residues as ball and sticks and the catalytic cysteine in yellow. The structure represents $HOIP_{CBR-C}$ from the ubiquitin complex and includes regions disordered in the apo form.

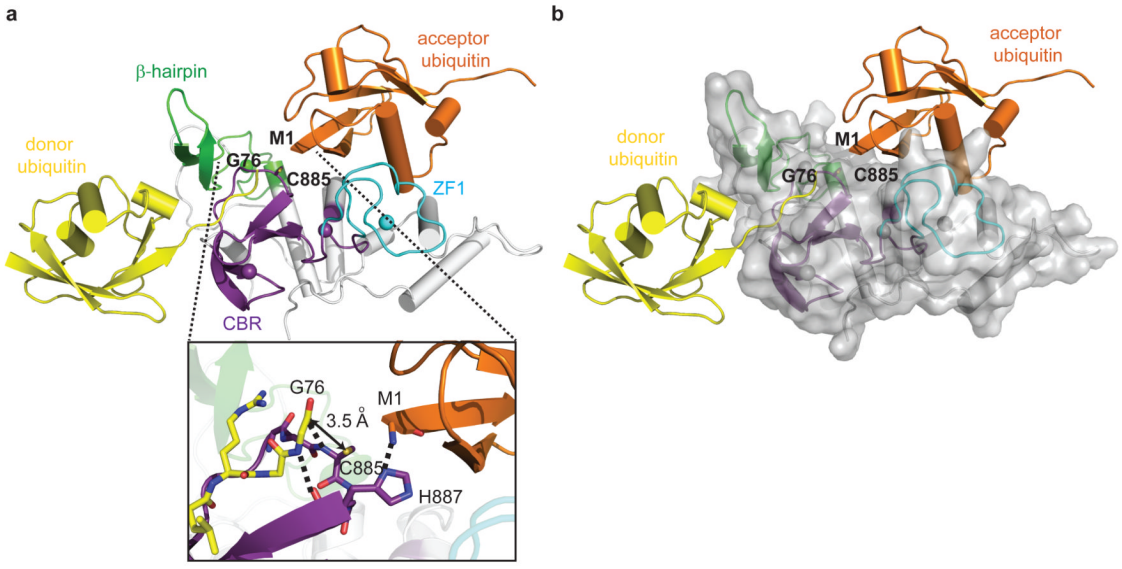

Fig. 2. The HOIP$_{CBR-C}$/ubiquitin transfer complex containing donor and acceptor ubiquitin

a, Ribbon representation of HOIP$_{CBR-C}$ in complex with the acceptor (orange) and donor (yellow) ubiquitin. HOIP$_{CBR-C}$ is shown in the same orientation as in Fig. 1e. The positions of C885, donor G76 and acceptor M1 are indicated. Insert, contacts made by HOIP$_{CBR-C}$ with donor and acceptor ubiquitin. The arrow shows the proximity between G76 of the donor and Sγ of C885. **b,** The HOIP$_{CBR-C}$/ubiquitin complex with HOIP$_{CBR-C}$ shown in a surface representation to emphasize the spatial relationship between the 3 molecules.

Europe PMC Funders Author Manuscripts

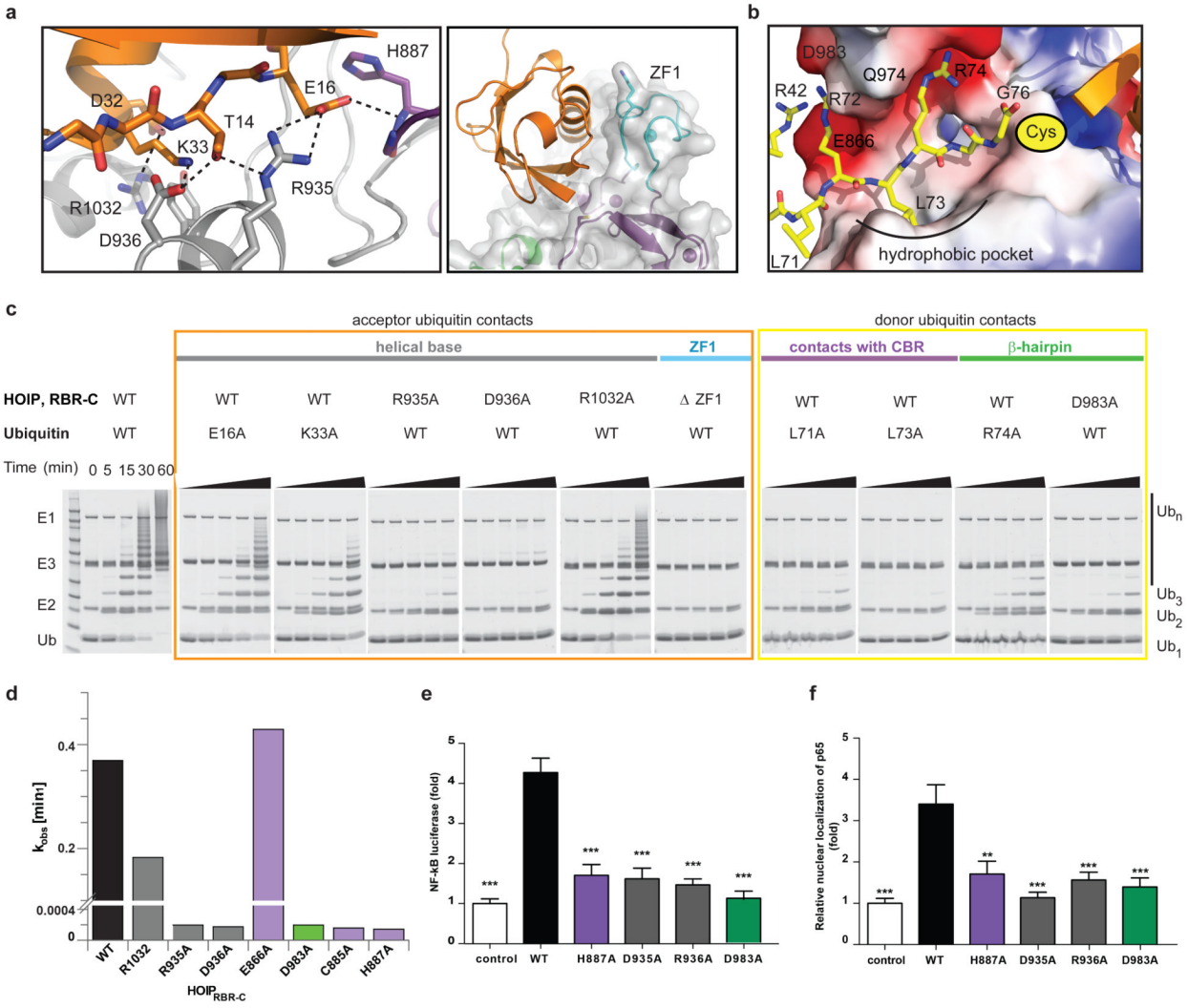

Fig. 3. Contacts between HOIP$_{CBR-C}$ and ubiquitin required for ubiquitin transfer

a, Close-up of the HOIP$_{CBR-C}$/acceptor ubiquitin interface focusing on the helical base and ZF1. **b,** Details of the HOIP$_{CBR-C}$/donor ubiquitin (yellow) interface. Positions of C885 and acceptor ubiquitin M1 are indicated. **c,** Steady-state ubiquitination assays. Mutants that target the acceptor interface are boxed in orange, those with donor in yellow. **d,** Single-turnover assays to determine the rate of tetraubiquitin formation. **e,** Luciferase assays showing that the NF-κB pathway is not efficiently activated by HOIP mutants H887A, R935A, D936A and D983A compared to WT. **f**, p65 translocations assay showing impaired p65 nuclear translocation upon expression of HOIP ligase-deficient mutants. Three independent experiments were performed using triplicate samples. Results were analyzed by ANOVA1 followed by Tukey post-tests. ** p<0.01; *** p<0.001 compared to wild-type HOIP.

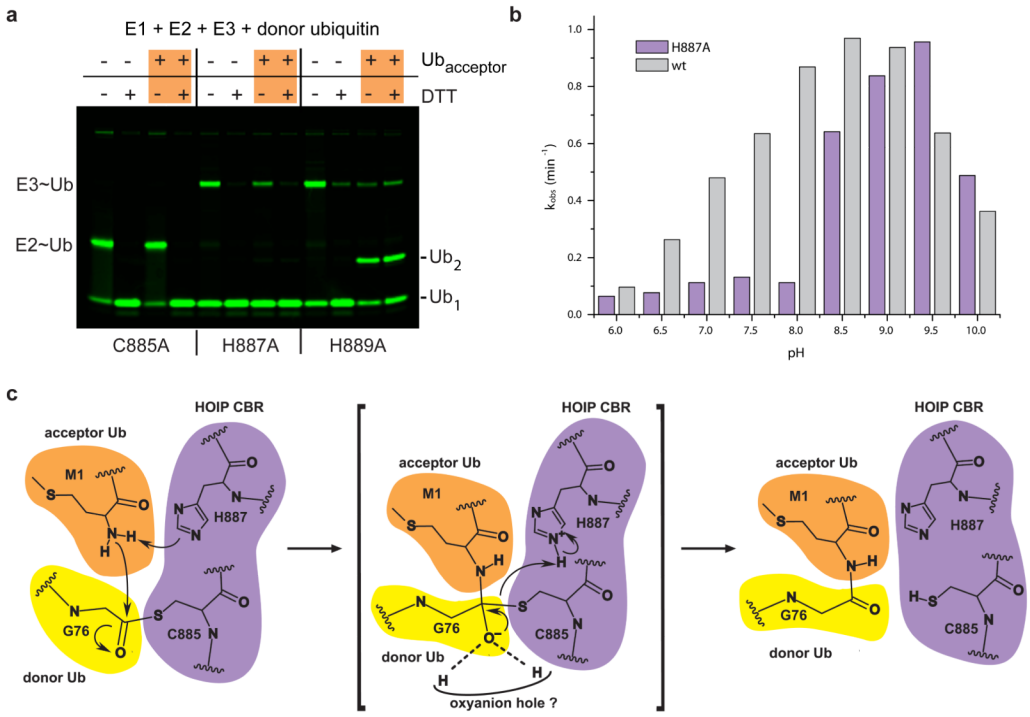

Fig. 4. HOIP H887 acts as the general base to activate the nucleophile

a, $HOIP_{RBR\text{-}C}$ H887A and H889A (which shows WT activity) mutants can form a thioester (lanes 1 and 2 of each mutant), indicating that neither residue is involved in transthiolation from E2 to E3. However, H887A has lost the ability to transfer to a substrate to form diubiquitin. An orange square indicates the presence of acceptor ubiquitin. **b,** Single-turnover assays of the pH-dependence of tetraubiquitin formation showing that the H887A mutant regains activity at higher pH at 25°C. **c,** Proposed mechanism for ubiquitin transfer by HOIP.

Europe PMC Funders Author Manuscripts